the FEBS Journal

Structural features and dynamics of a cold-adapted alkaline phosphatase studied by EPR spectroscopy

Pétur O. Heidarsson*, Snorri Th. Sigurdsson and Bjarni Ásgeirsson

Department of Biochemistry, Science Institute, University of Iceland, Reykjavik, Iceland

Keywords
alkaline phosphatase; catalytic mechanism; electron paramagnetic resonance; protein dynamics; site-directed spin-labeling

Correspondence
B. Ásgeirsson, Department of Biochemistry, Science Institute, University of Iceland, Dunhaga 3, IS-107 Reykjavik, Iceland
Fax: +354 552 8911
Tel: +354 525 4800
E-mail: bjarni@raunvis.hi.is

***Present address**
Structural Biology and NMR Laboratory (SBiN Lab), University of Copenhagen, Denmark

(Received 20 December 2008, revised 6 February 2009, accepted 9 March 2009)

doi:10.1111/j.1742-4658.2009.06996.x

EPR spectroscopy, performed after site-directed spin-labeling, was used to study structural dynamics in a cold-adapted alkaline phosphatase (EC 3.1.1.1). Differences in the structural environment of six spin-labeled side chains allowed them to be classified (with reference to previously obtained mobility maps) as belonging to loop positions (either relatively surface exposed or in structural contact) or helix positions (surface exposed, in contact, or buried). The mobility map constructed in the present study provides structural information that is in broad agreement with the location in the crystal structure. All but one of the chosen serine-to-cysteine mutations reduced activity considerably and this coincided with improved thermal stability. The effect of spin-labeling on enzyme function ranged from non-perturbing to an almost complete loss of activity. In the latter case, treatment with a thiol reagent reactivated the enzyme, indicating relief of steric hindrance to the catalytic process. Two mutations of an active-site residue W274 (K328 in *Escherichia coli* alkaline phosphatase), known to reduce activity and increase stability of *Vibrio* alkaline phosphatase, gave a coincidental reduction in mobility of a nearby spin-label located at C67, as determined by EPR spectroscopy. This suggests that movement of the helix carrying C67 and the closely positioned nucleophilic S65 is interconnected with catalytic events.

Protein function depends on dynamic motions. The available information regarding such events is important for our understanding of enzyme catalysis, particularly because conformational movements may often comprise the rate-limiting step [1]. However, the experimental assessment of polypeptide flexibility in solution is generally difficult [2]. Movements of individual atoms cannot be measured in real time, except in special cases. Protein dynamics must, therefore, be inferred from various biophysical measurements performed on the ensemble of molecules containing various substates in equilibrium, with the relative population of each state depending on the experimental conditions. A number of methods have been employed to evaluate protein dynamics, in addition to NMR [3–5], including hydrogen-deuterium mass spectrometry [6,7], molecular dynamics simulations [8] and fluorescence spectroscopy [9]. Mobile surface accessible parts, such as flexible loops, are often involved in the catalytically important structural dynamics [10–13]. Therefore, identifying mobility and tertiary interactions, in addition to any interactions amongst more buried residues, should prove to be very informative with regard to enzyme function.

In recent years, EPR spectroscopy has emerged as a powerful tool for studying protein structure and dynamics in conjunction with site-directed spin-labeling (SDSL) [14–16]. A cysteine side chain is introduced into the protein structure with site-directed mutagenesis and is subsequently chemically modified with

Abbreviations
AP, alkaline phosphatase; MTSSL, methanethiosulfonate spin-label.

a nitroxide radical. The most commonly used nitroxide radical is the methanethiosulfonate spin-label (MTSSL), which, upon attachment to a cysteine, yields the spin-labeled side chain, commonly termed R1 [16,17]. The dynamical modes of the nitroxide are a combination of rotary diffusion of the macromolecule, internal bond isomerization of the spin-label and backbone fluctuations. Analysing the lineshape of the resulting EPR spectrum of R1 can reveal detailed information about the protein, such as secondary and tertiary structural interactions, as well as dynamic modes at the spin-labeled site [18]. In addition, by using double labeling, distances as long as 80 Å have been measured using pulsed double resonance EPR methods (e.g. pulsed electron-electron double resonance, double electron electron resonance) [19]. By combining distance and lineshape measurements, global information can be obtained and the structure of whole domains can be determined [20], with one example being lipid-embedded protein channels [21]. We were interested in applying EPR to study local protein environments in a cold-active enzyme.

Alkaline phosphatase (AP) (EC 3.1.1.1) from the marine *Vibrio* sp. G15-21 is a cold-adapted phosphomonoesterase [22]. The recently solved crystal structure shows a dimeric form, which is a characteristic of all known AP structures [23]. Many cold-adapted enzymes have reduced thermal stabilities as a result of an altered pattern of stabilizing weak noncovalent interactions. Consequently, cold-adaptation of enzymes is commonly considered to be the result of an enhanced structural flexibility [24–26]. This increased flexibility might be global or confined to selected areas of functional importance, such as the active site or ligand binding sites [27]. As a result, cold-adapted enzymes provide an opportunity to detect experimentally more decisive movements than in the more heat-tolerant variants.

The catalytic mechanism of AP goes through a covalent serine-phosphoryl intermediate, in which two zinc ions first promote substrate polarization and nucleophile activation by electrostatic interactions, and then aid in the hydrolysis of the covalent intermediate through the generation of a hydroxide ion. The magnesium ion may be involved directly in the latter step as a general base catalyst [28] or stabilize the transfers of the phosphoryl group in the transition state [29]. The mobility of the active site during the catalytic cycle, collectively or bound to individual residues, remains uncharted. Early kinetic experiments suggested that a conformational change might be a rate-determining step under certain conditions [30]. Although many studies have shown that subunit interactions affect catalytic efficiency in APs, presumably by shaping the exact positioning and mobility of key residues, a lack of information about the nature of such movements leads to their exclusion from present models.

In the present study, we used site-directed spin-labeling of the *Vibrio* AP in conjunction with EPR to elucidate features of structural dynamics at selected sites. Specifically, the mobility of the spin-label was used to identify motional constraints of secondary structural elements and to probe tertiary interactions. First, we selected residues that are close to the active site according to the crystal structure, both in helices and loops [23]. Using a spin-labeled native cysteine, we measured local structural changes induced by both a denaturant and by mutating an important active site residue. Second, we engineered cysteines to place the spin-label at sites in two inserts unique to the *Vibrio* AP polypeptide sequence [23] aiming to obtain information about their possible tertiary interactions and change in mobility. Third, we used EPR to examine the mobility of a cysteine placed by mutagenesis at a location where disulfide bridge formation with the native C67 was previously successful [31], despite a crystal structure distance of 12 Å. We demonstrate that EPR spectra of spin-labeled variants can be used to extract information on local dynamics of the various secondary backbone structures and some tertiary interactions in this cold-adapted enzyme.

Results

Selection of spin-labeled sites and active-site mutations

Native *Vibrio* AP has one cysteine residue (C67) that is positioned close to the nucleophilic S65 (equivalent to S102 in *Escherichia coli* AP) (Fig. 1). Our strategy was to change C67 to a serine and then individually spin-label other residues by mutations to a cysteine followed by reaction with a spin-labeling reagent (Fig. 1) to assess the local dynamics. All cysteine mutations were generated from serine residues to ensure minimal perturbation in the atomic configuration (i.e. isosteric replacement of a hydroxyl group of serine for a thiol group of cysteine). Previously, nearby loop-residues S53, S78 and S80 were all predicted by a homology model to be within disulfide bridge bonding distance of C67. The mutation of S53 to cysteine resulted in the formation of a disulfide bridge with C67, whereas mutations S78C and S80C did not [31]. The recently solved crystal structure [23] has shown, however, that the shortest distance between the S53 hydroxyl and C67 thiol is 1.2 nm, suggesting that some loop

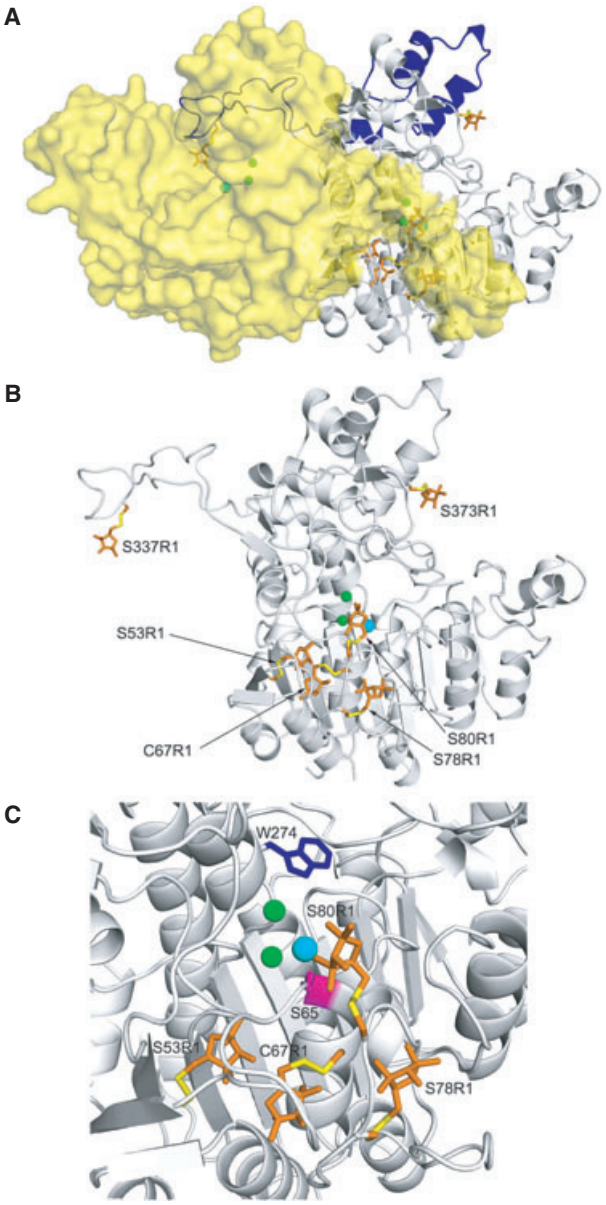

Fig. 1. The structure of *Vibrio* AP (Protein Databank accession number 3E2D) [23]. (A) The dimeric form. The active sites are indicated by the positions of the metal ions (two zincs in green and magnesium in cyan). The large insert that characterizes *Vibrio* AP is shown in blue. (B) One subunit of the AP dimer showing the spin-labeled sites. The spin-labeled sites comprised S53, C67, S78, S80, S337 and S373. The other subunit binds to the left of the subunit shown and in front of the surface loop carrying S337. (C) Close-up view. The nucleophilic serine is shown in purple and the active site residue W274 is shown in blue. The two small spheres are the zinc ions and the single larger sphere is the magnesium ion. The image was created with PYMOL, version 1.1 [49].

movement must take place in solution to close a disulfide bond between these two residues. Thus, we decided to probe mobility in these areas. We also chose to place the spin-label within two insert regions unique to the cold-active *Vibrio* AP, by introducing mutations S337C and S373C [32,33]. S337 is situated on an extended loop structure (Fig. 1) that reaches from one monomeric subunit around the other subunit, partly covering its active site. On the other hand, S373 resides on a solvent-exposed α-helix in proximity to the active site. Finally, to determine whether an amino acid that was important for activity had any effect on the mobility of residues close to the active site (i.e. specifically at the helix carrying C67), we mutated W274 to either a lysine (analogous to *E. coli* AP) or a histidine (analogous to mammalian APs). The spin-label was placed at residue 67 in both cases. Studies on *E. coli* AP have shown that K328 (W274 in *Vibrio* AP) is important for both activity and active site stability [32,33].

Kinetic properties and temperature stability

The activity and stability of the *Vibrio* AP was measured for each mutation, before and after spin-labeling. Furthermore, the activity and stability of the spin-labeled proteins was also determined. Table 1 shows the kinetic and thermodynamic properties of the wild-type (WT) AP compared with WT*, which contains a serine replacement of the native C67, and their spin-labeled derivatives.

Replacing the WT C67 with serine reduced k_{cat} by over 40% and resulted in a large increase in T_m by 5.1 °C, leaving K_m relatively unchanged. The k_{cat}/K_m values were 18.0 and 10.0 $s^{-1}\cdot M^{-1}$, respectively. Both W274 variants displayed lower catalytic efficiency (k_{cat}/K_m) than WT, along with increased resistance toward urea inactivation (see below), whereas global stability as judged by T_m was only increased in the case of the W274K variant (Table 1).

All the cysteine for serine mutations introduced into WT*, except S53C, caused a rather large change in both activity and stability, in particular after spin-labeling (Table 1). The global stability (T_m), measured by CD, was increased in WT* variants S78C, S80C, S337C, and S373C, whereas S53C was not changed compared to the C67S control. k_{cat} values were similarly reduced to approximately 10–20% of the control value, except for the S53C variant, which remained unchanged. The K_m values in the cysteine variants were of similar order as in the C67S control or the C67 WT enzyme. The spin-labeling had minor effects on heat-stability. The T_m was 0.7–0.8 °C lower for C67R1 (WT) and S373R1, whereas the decrease was over twice that for S78R1, S80R1 and S337R1. By contrast, S53R1 spin-labeled protein has a slightly higher T_m (0.9 °C) than the WT. The attachment of

Table 1. Activity and T_m values for WT *Vibrio* AP (WT) and variants with and without spin-label. Kinetic parameters were determined in 0.1 M Caps, 1.0 mM $MgCl_2$, pH 9.8, with *p*-nitrophenyl phosphate at a concentration in the range 0.01–0.5 mM. Percent activity of variants after spin-labeling with MTSSL and the effects of spin-labeling on T_m were measured by the standard transphosphorylating assay and CD spectroscopy, respectively. ΔT_m is the difference between spin-labeled and nonspin-labeled variants, where a negative value denotes reduced stability. ND, not determined.

	Without MTSSL				With MTSSL	
Enzyme variant	k_{cat} (s^{-1})	K_m (mM)	k_{cat}/K_m ($s^{-1}\cdot M^{-1}$) × 10^{-6}	T_m (°C)	Activity (%)	ΔT_m (°C)
C67 (WT)	775 ± 42	0.043 ± 0.008	18.0	50.5 ± 0.2	95	−0.7
W274K	242 ± 45	0.041 ± 0.009	5.9	52.5 ± 0.3	94	ND
W274H	368 ± 30	0.049 ± 0.004	7.5	49.7 ± 0.3	95	ND
C67S (WT*)	448 ± 68	0.039 ± 0.007	10.0	55.6 ± 0.4	[a]	[a]
S53C	497 ± 50	0.048 ± 0.004	10.4	55.5 ± 0.5	105	+0.9
S78C	95 ± 12	0.026 ± 0.005	3.7	57.2 ± 0.5	1.5	−1.6
S80C	89 ± 16	0.025 ± 0.005	3.6	57.0 ± 0.3	2.5	−1.9
S337C	41 ± 5	0.078 ± 0.007	0.5	57.5 ± 0.5	91	−2.5
S373C	50 ± 14	0.041 ± 0.004	1.2	60.6 ± 0.3	88	−0.8

[a] Not spin-labeled.

the spin-label reduced the activity of the S78C and S80C loop-variants by 97–99% of their previous activity, whereas no effect on activity was observed for S53C, and a modest 12% drop in activity was observed for S337C and S373C. The activity of the two W274 variants was not affected by spin-labeling at C67 beyond the small decrease observed in the control.

Characterization of mobility by EPR spectroscopy

Figure 2 shows the EPR spectra of the spin-labeled native C67 and the other serine-to-cysteine variants. The EPR spectra showed two distinct components that are especially apparent in the low field end of the spectra. These components correspond to two different populations of the nitroxide spin-label that have different rotameric forms of the R1 side chain [34]. An immobile rotamer is suggested to arise because of an interaction of the probe with other parts of the protein, whereas the more mobile component lacks this interaction. The spectrum of S80R1 most clearly showed a two-population system (Fig. 2, arrows). Rotational correlation times were calculated for both components in each spin-labeled variant, indicated as $\tau_R{}^m$ and $\tau_R{}^i$ for the mobile and immobile components, respectively (Table 2). The scaled mobility factor (M_s) is also shown in Table 2 because it has been shown to reflect backbone dynamics most accurately [35]. M_s values, calculated using the central peak width, indicated that S78R1 and S80R1 had relatively high mobility, with M_s equaling 0.62 and 0.65, respectively, whereas S53R1 and S373R1 were amongst the most immobile residues with M_s equaling 0.42 and 0.45, respectively. S78R1 and S80R1 also showed the highest τ_R in both the mobile and immobile components, whereas S53R1 and S373R1 showed similar low mobility. C67R1 had a predominantly immobile component, with a minor mobile component of $\tau_R{}^m$ = 2.96 ns (Fig. 2), whereas the scaled mobility factor, M_s, was intermediate between S53R1 and S78R1 or S780R1. The effect of the two mutations on mobility of the C67R1 was very clear on M_s, whereas the τ_R values were practically unchanged (Table 2). As expected, S337R1 displayed high mobility, with the highest M_s value of 0.74 and the shortest $\tau_R{}^m$ of 2.85 ns. Interestingly, however, a minor component in the S337R1 spectra with a $\tau_R{}^i$ of 6.55 ns was also observed, which corresponds to an immobilized state.

The native *Vibrio* AP C67 is in close proximity to the catalytic S65 and on the same helix. Therefore, we decided to determine the effects of urea on the mobility of C67R1 by EPR spectroscopy and compare that with the loss of enzyme activity (Fig. 3). Total loss of activity was accomplished at lower urea concentration (< 1.5 M) than was needed to confer maximal rotational freedom of C67R1 (> 2.0 M) as measured by us. The ratio of the mobile to the immobile component of the low field spectrum (Fig. 3A, arrows) increased with increased urea concentration, indicating a shift in the equilibrium towards the more mobile rotamer.

Figure 4 shows the effect of temperature on the probe mobility in WT *Vibrio* AP and the two W274 mutants. The variant C67R1/W274K showed greater immobilization than C67R1/W274H, with a reduced M_s value of 20% on average, compared to C67R1 in the temperature range 278–298 K (Fig. 4A). Figure 4B shows the effect of urea on the activity of the WT and

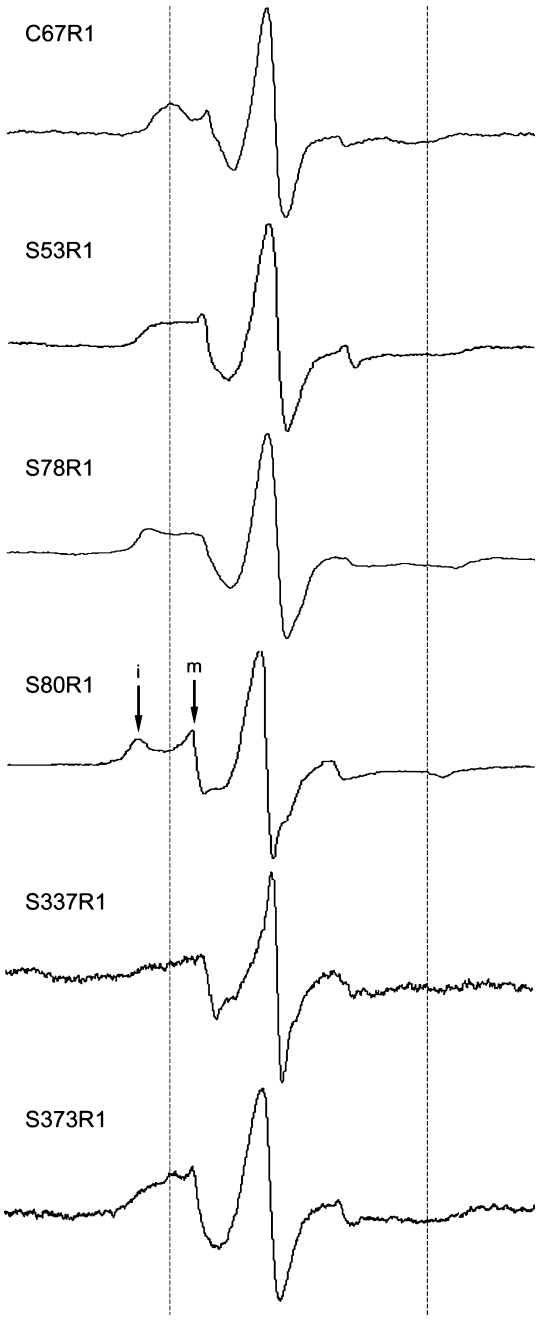

Fig. 2. EPR spectra of the spin-labeled cysteine variants. The dotted lines indicate the spectral width of WT C67R1 and are intended to aid the eye with respect to detecting spectral broadening. The splitting of the leftmost peak into an immobile component (i) and a mobile component (m) is indicated and is most revealing for the state of the spin-label.

W274 variants, along with the calculated Gibbs free energy values for unfolding [36]. The two variants both showed increased active site stability compared to the WT, with the W274K variant being more stable.

Table 2. The scaled mobility factor (M_s) and rotational correlation times (τ_R) for the spin-labeled cysteine variants. The values of τ_R were calculated for both the mobile (τ_R^m) and immobile (τ_R^i) spectral components. From experiments with C67R1 that were performed up to four times under identical conditions, the error estimate was better than 6%.

Variant	M_s	τ_R^m (ns)	τ_R^i (ns)
C67R1	0.56	2.96	5.94
C67R1/W274K	0.44	2.95	5.95
C67R1/W274H	0.48	2.93	5.96
S53R1	0.42	3.20	5.48
S78R1	0.62	3.57	11.3
S80R1	0.65	3.60	14.1
S337R1	0.74	2.85	6.55
S373R1	0.45	2.92	6.33

Discussion

In the present study, we examined the structural and dynamical features of a cold-adapted AP using site-directed spin-labeling in conjunction with EPR spectroscopy. The effects of cysteine mutations and spin-labeling on kinetic properties and stability were also studied. Replacing C67 with serine (designated WT* in Table 1) reduced the catalytic efficiency (k_{cat}/K_m) by 45% and increased temperature stability (T_m) of the enzyme by 5 °C. Replacing C67 with alanine resulted in an almost identical drop in activity as that caused by C67S, along with an increase in stability (data not shown). Because this residue is not involved in the chemical step and is positioned outside the active site, it might be considered to influence the flexibility in the WT enzyme through stability reduction by an as yet unknown mechanism, giving it an auxiliary functional role. The substrate binding cavity was apparently structurally unaltered as determined by an almost unchanged K_m. All the cysteine-for-serine mutations introduced into WT* AP, except S53C, caused rather large deviations from the control, where an increased thermal stability accompanied a large drop in k_{cat} (Table 1). The subsequent introduction of the spin-label onto side chains C67, S53C, S337C and S373C had little effect on catalytic rate of respective controls. Furthermore, the thermal stabilities of the C67, S53C and S373C variants were scarcely changed by the spin-label, indicating that these positions are solvent-exposed. The unexpected and dramatic activity reduction of the S78C and S80C loop-variants (97–99%) after spin-labeling suggests that the area around the loop carrying residues 78–80 is important for correct functional geometry and/or movement of the catalytic site. Figure 1 shows how close the loop

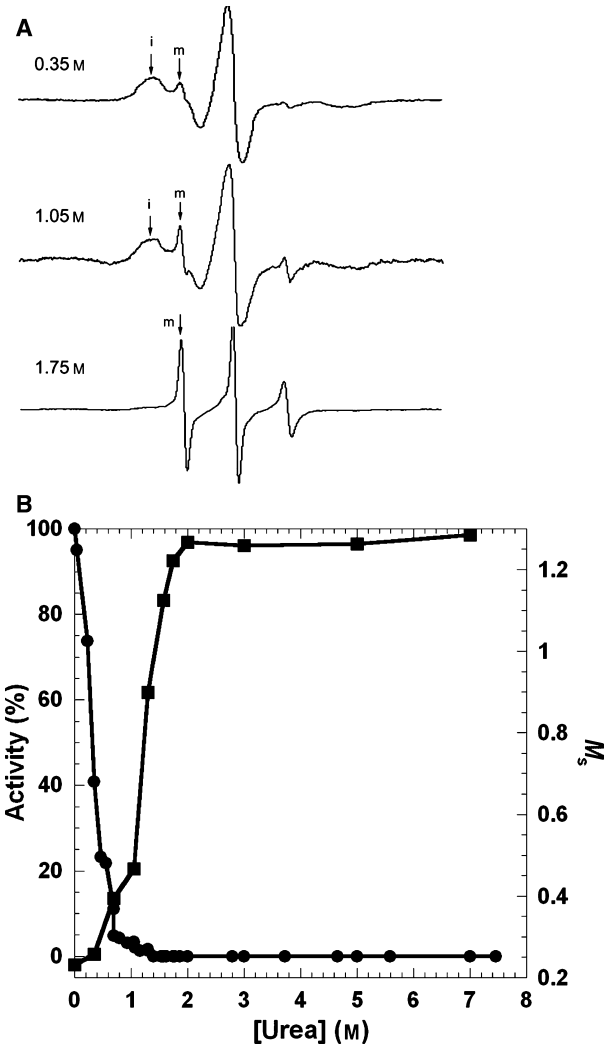

Fig. 3. (A) EPR spectra of C67R1 measured in different concentrations of urea. C67R1 samples were incubated in 25 mM Mops, 1.0 mM $MgSO_4$, pH 8.0, in different concentrations of urea for 4 h before measuring the EPR spectra. Mobile and immobile components are indicated with arrows. (B) Change in activity (●) and C67R1 mobility (■) with urea concentration. The activity in the standard assay and EPR spectra of the spin-labeled WT AP were measured after incubation in urea. The scaled mobility factor (M_s) was calculated from the central linewidth of the EPR spectra.

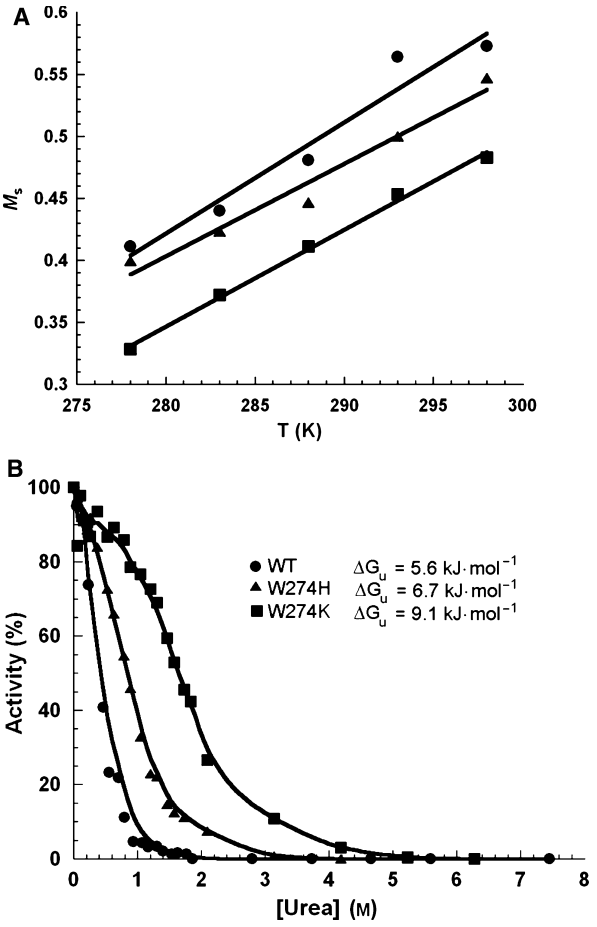

Fig. 4. (A) M_s values for C67R1 (●), C67R1/W274K (■) and C67R1/W274H (▲). Values were calculated from spectra measured in 20 mM Tris, 10 mM $MgCl_2$, pH 8.0. (B) Dependence of activity on urea concentration in the WT AP and active site variants. The activity was measured after incubation in urea using the same conditions as those employed in Fig. 3A. $\Delta G_u(H_2O)$ values were calculated using the linear-extrapolation method [36].

packs against the helix, where the nucleophilic S65 is in an apical position. The S80 position allows the nitroxide spin-label placed there to point into the active site close to the S65 and in the direction of the metal ions. An almost complete reactivation of S78R1 and S80R1 variants upon incubation with dithiothreitol was achieved within 3 h (data not shown). This observation supports the idea that wedging the spin-label into the structure at functionally sensitive positions was the cause of the structural malfunction and demonstrates the possible use of MTSSL as a molecular switch. The spin-label has been shown to perturb function and stability of other enzymes to a different extent depending on the location of the residue to which it is attached [18]. Generally, spin-labeling residues close to the active site, or those involved in substrate binding, were the only cases shown to cause any significant reduction in activity for solvent-exposed sites. Spin-labeling of buried residues does, however, often lead to complete loss of activity and a severe destabilization [18].

Figure 5 shows the mobility map for six different spin-labeled sites of *Vibrio* AP, as well as for the two C67R1/W274 variants. It has reference areas based on previous work by Isas *et al.* [37] who constructed a

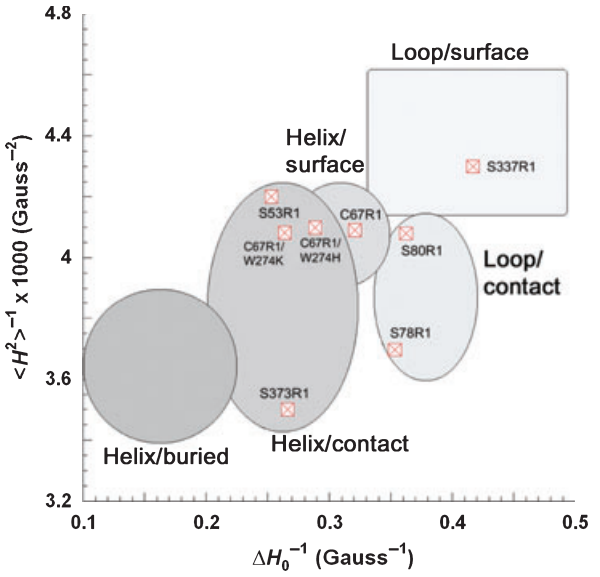

Fig. 5. Locational analysis of spin-labeled sites by EPR spectra. Mobility map for *Vibrio* AP based on the map reported by Isas *et al.* [37] showing the reciprocal of the second moment ($<H^2>$) versus the reciprocal central linewidth (ΔH_0). The variants C67R1/W274K and C67R1/W274H are also shown.

mobility map based on a detailed study of thirty spin-labeled sites of annexin-12. It was concluded that the mobility of R1 reflected the secondary and tertiary structural environment at the spin-labeled sites, and this has subsequently been validated for other proteins [38,39]. The ΔH_0^{-1} parameter gives an indication about movement of the point where the spin-label attaches to the backbone of the polypeptide, whereas the $<H^2>^{-1}$ parameter also gives a measure of the spatial freedom for the conical movement of the nitroxide ring [15].

The mobility of the probe at position C67 was located within the helix/surface region on the plot, whereas the mobility characteristics of S53R1 and S373R1 indicated a less mobile helix/contact site for these two positions. It should be noted, however, that their placements in the plot were at the opposite extreme parts of that region shown in Fig. 5. S53R1 demonstrated a much higher value of $<H^2>^{-1}$ than S373R1, despite being in one of the most buried positions of the sites tested (Fig. 1). This might indicate an unexpected freedom of S53 side-chain mobility as a result of local breathing motions, whereas S373 may be experiencing tertiary interactions that are not immediately obvious from Fig. 1. Our previous results showed that a disulfide bond was formed between S53C (but not from S78C or S80C) and the native C67 [31], despite the unfavorable distance as determined by the crystal structure. This emphasizes that EPR measurements do not reveal anything about the available distance that the probe might move within. S337R1, a residue chosen for its position on the large nonstructured loop that embraces the opposite monomer, fell onto the mobility plot in the loop/surface region as expected.

The map positions of S78R1 and S80R1 in Fig. 5 came within the loop/contact regions of the map, which indicates a somehow restricted motion as a result of interaction with other parts of the protein. Spin-labeling and EPR spectroscopy confirmed that the loop region 78–80 has high mobility in the ΔH_0^{-1} dimension (backbone movement), although the 78 side chain had a relatively low mobility in the $<H^2>^{-1}$ dimension. Given the results for S78C and S80C with respect to inactivation by spin-labeling, it may be suggested that these spin-labels could affect the mobility of S65-carrying helix, rendering the nucleophile less active, or, in the case of S80R1, suppress the formation of the catalytic alkoxide ion by pointing the nitroxide toward the nearby enzyme active site.

The mobility of C67R1 puts this residue inside the well-defined helix/surface mobility region of the plot. It is well established that R1 mobility on solvent-exposed helices predominantly reflects backbone dynamics [35]. C67 does have relatively high mobility, which might indicate high mobility for the backbone attachment of the nucleophilic S65 as well (being close on the same helix). From the crystal structure, it can be seen that C67 and S373 are in helical positions most likely to have the spin-label oriented into the solvent, rendering it at least partially solvent accessible. The effect of urea denaturation on C67R1 mobility observed in the present study is consistent with previous results obtained using fluorescence spectroscopy [40], where urea denaturation of WT *Vibrio* AP was monitored using tryptophan fluorescence and kinetic measurements. Similar to the findings obtained in the present study, the loss of activity occurred at less than 1 M urea, before a significant change in global structure was observed with fluorescence spectroscopy (1–3 M). Early inactivation may coincide with loss of the magnesium ion from the active site as a result of increased mobility of the binding ligands [40]. To determine whether magnesium removal under native conditions could affect the mobility of C67R1, the EPR spectrum of the spin-labeled variant was measured without adding Mg^{2+} to the buffer. As expected, the EPR spectrum displayed some degree of protein denaturation, which was observed as a narrow mobile component (data not shown). This would signal the expected stability reduction by magnesium removal.

However, the overall spectral width reflected in τ_R and the M_s factor did not show any significant difference compared to the C67R1 spectrum with magnesium ions present. This indicated that the mobility around C67 is not influenced by the potential presence or absence of a magnesium ion in the third metal binding site that the W274 mutation-target is part of.

The active site mutations of W274 were performed to elucidate any link between the reduction in activity observed for the W274 variants [40] and the measured mobility of C67R1. Studies on *E. coli* AP have shown that the residue equivalent to the *Vibrio* AP W274 is important for both activity and active site stability [32,33]. Both *Vibrio* AP variants displayed lower catalytic efficiency (k_{cat}/K_m) as well as increased resistance toward urea inactivation (Fig. 3B), which is an indication of greater rigidity in the active site. Thus, replacing W274 with histidine, a residue analogous to mammalian APs, could be expected to reduce activity as a result of reduced movement in or around the active site, which is exactly what is observed with respect to the mobility of C67R1. An even greater reduction in C67R1 mobility was observed when the residue was replaced with lysine, analogous to *E. coli* AP. A distance of more than 17 Å separates these two positions according to the crystal structure, excluding the possibility of a direct steric interaction between the spin-label and the side chain at position 274. The results of the EPR indicate a reduction in the rate of movement of the R1 attachment-point (ΔH_0^{-1} component in Fig. 1), with little change being observed in side-chain/R1 conical mobility (i.e. the $<H^2>^{-1}$ component). This would be consistent with facile movement of Ser65 as a factor promoting catalysis because it is on the opposite side of the helix carrying C67R1 (Fig. 1).

The presence of additional loop regions in *Vibrio* AP compared to other APs raises questions about their relevance for cold-adaptation. The mobility of residue S337, positioned on the large loop that embraces the opposite monomer, mapped to the loop/surface region of the mobility plot. This was expected and suggests that this loop is quite free to move, perhaps making movements at the monomer contact in the dimer more facile. By contrast, the relative immobility of the spin-labeled site S373R1 observed in the mobility map indicated a more stable tertiary interaction of that residue with other parts of the protein, despite the crystal structure indicating that the spin-label should be situated on a solvent-exposed helix. One explanation might be that the region containing the spin-labeled site can move in solution, and thereby bring S373R1 closer to other residues in the area where the active site opens. Such tertiary interactions could explain the slow-moving component in the EPR spectrum. Indeed, two-component spectra, as observed for S373R1 in the present study, might arise from two states of the protein in equilibrium, as observed with spin-labeled hemoglobin [41]. On the other hand, the observed EPR immobility component of the S373R1 probe might involve a fortuitous interaction between the nitroxide ring and nearby loops or the residue at $i + 1$ or $i + 4$ in the same helix, which are glutamate and lysine, respectively. The degree of this interaction, which is modulated by the identity of the interacting residue, has been shown to affect the motion of R1 [42]. Further spin-labeling experiments could reveal where these interactions originate from, either by mutation of the possibly interacting residues or by using double site-directed spin-labeling for distance measurements between the insert region and a likely interacting site.

In conclusion, in the present study, we have demonstrated that the helix on which the nucleophilic serine in *Vibrio* AP is positioned has a different mobility depending on which residue is in position 274 inside the active site. The placement of the spin-label on two separate residues in a loop adjacent to the helix stopped enzymatic activity, despite the fact that these are surface locations. Thus, dynamic movement of this loop appears to determine the efficiency of the active-site. The results obtained indicate that the EPR technique can be employed to monitor local changes in backbone mobility that are relevant to the catalytic reaction pathway in APs.

Experimental procedures

Cloning and mutagenesis

The *Vibrio* AP gene was amplified by standard PCR methods from the pBAS20 (pBluescript KS+; Stratagene, La Jolla, CA, USA) plasmid [40] and transferred into the pASK-IBA3plus vector (IBA, Göttingen, Germany), which contains a region encoding the eight amino acid Strep-Tag II affinity peptide (WSHPQFEK). An additional nine amino acid spacer connecting the AP sequence [43] with the Strep-Tag originated from the multiple cloning site when using *Eco*RI and *Pst*I restriction sites (LQGDHGLSA). Cysteine variants were constructed with the QuikChange® kit (Stratagene) according to the manufacturer's instructions. Oligonucleotide primer pairs for mutagenesis were synthesized by TAG (Copenhagen, Denmark). All plasmids were cloned and propagated in DH5α cells grown on LB agar plates containing ampicillin. Plasmids were isolated using Qiaprep Spin Miniprep kit (Qiagen, Hilden,

Germany). The nucleotide sequences were verified by sequencing the entire gene.

Expression and purification

Competent *E. coli* cells of strain LMG194 (Invitrogen, Carlsbad, CA, USA) were transformed with plasmids containing the WT *Vibrio* AP gene or with desired mutations. A preculture was grown in 100 mL of LB medium supplemented with 100 $\mu g \cdot mL^{-1}$ ampicillin at 37 °C for 4 h and this culture was then transferred into 4.5 L of the same medium at pH 8.0 and divided into 9×0.5 L portions. The cell culture was incubated at 20 °C on an orbital shaker until D_{550} of 0.6 was reached. Anhydrotetracyclin was used to induce expression at a final concentration of 20 $ng \cdot mL^{-1}$ and the temperature was lowered to 18 °C during that period. The cell culture was allowed to reach a stationary phase before harvesting.

The cells were pelleted by centrifugation for 10 min at 10 000 ***g*** and 4 °C using a Sorvall RC5C centrifuge (Sorvall Inc., Norwalk CT, USA). The cell pellet was redissolved in 400 mL of 20 mM Tris, 10 mM $MgCl_2$, 0.01% Triton X-100, 0.5 $mg \cdot mL^{-1}$ lysozyme at pH 8.0, and left to stand at 4 °C for 5 h before being frozen at −20 °C. For enzyme purification, the crude protein solution was thawed and left to stand for 30 min at room temperature after DNAase had been added to a final concentration of 0.05 $mg \cdot mL^{-1}$. The solution was then centrifuged at 10 000 ***g*** for 20 min. The clear supernatant containing active *Vibrio* AP was applied to a streptactin affinity column that recognizes and binds the Strep-Tag affinity peptide. After binding of AP, the column was washed with five column volumes of 20 mM Tris, 10 mM $MgCl_2$, 150 mM NaCl, pH 8.0, 15% ethylene glycol. Bound protein was eluted with 2.5 mM desthiobiotin in the same buffer without NaCl. The purified protein was frozen in liquid nitrogen and stored at −20 °C. The purity of all proteins was confirmed > 95% by SDS/PAGE. Protein concentration was determined using a Coomassie Blue assay [44], or by using a calculated extinction coefficient [45].

Enzyme kinetics and stability

Enzyme activity was routinely measured under transphosphorylating conditions with 5 mM *p*-nitrophenyl phosphate in 1.0 M diethanolamine, 1.0 mM $MgCl_2$, pH 9.8 at 25 °C. The enzyme reaction was initiated by addition of enzyme to the pre-heated assay medium and the release of *p*-nitrophenol monitored at 405 nm (extinction coefficient 18.5 $mM^{-1} \cdot cm^{-1}$). Kinetic rate constants were determined under hydrolysing conditions in 0.1 M Caps, 1.0 mM $MgCl_2$, pH 9.8, at 25 °C with six different substrate concentrations in the range 0.01–0.5 mM. The turnover number (k_{cat}) was calculated per monomer mass.

Global thermal stability of secondary structures was assessed by measuring circular dichroism using a 2 mm cuvette in a Jasco 810 CD spectrometer (Jasco, Tokyo, Japan). Samples were measured in 50 mM Mops, 1.0 mM $MgSO_4$, pH 8.0. The CD signal at 222 nm was measured with a temperature increase of 1 $°C \cdot min^{-1}$ in the range 20–90 °C. The protein concentration was 0.05–0.1 $mg \cdot mL^{-1}$.

For determination of the effects of denaturation on inactivation and EPR spectra, samples were incubated for 4 h at 15 °C in a 25 mM Mops, 1.0 mM $MgSO_4$, pH 8.0 solution containing different concentrations of urea. Remaining activity was measured using standard protocol at 25 °C.

Spin-labeling and EPR measurements

Vibrio AP and variants (in elution buffer) were typically incubated with a 10-fold excess of (1-oxy-2,2,5,5-tetramethylpyrrolinyl-3-methyl)-methane thiosulfonate spin-label (MTSSL; Toronto Research Chemicals, North York, Canada). The reaction was allowed to proceed at 20 °C for 30 min and then at 4 °C for 2–4 h or overnight. Unreacted spin-label was removed from the solution using a Sephadex G-25 gel filtration column equilibrated with 20 mM Tris, 10 mM $MgCl_2$, pH 8.0, and the protein solutions were subsequently concentrated to 150–200 μM using a Millipore Ultracel YM-30 concentrator (Millipore, Billerica, MA, USA) with 30 kDa cut-off.

All spectra were aquired on an EPR X-band MiniScope MS-200 spectrometer (Magnettech, Berlin, Germany). Protein samples (approximately 10 μL) were loaded into capillaries, inserted into the resonator, and EPR spectra collected at 1 G modulation amplitude, 2 mW microwave power, 120 G sweep, at 20 °C. Unless otherwise stated, spin-labeled protein samples contained 30% (w/w) sucrose to increase viscosity and thus minimize contributions from protein tumbling in the EPR spectra [18].

M_s has been shown to be an accurate measure of R1 mobility [35]. M_s takes values in the range 0–1 for a fully restricted probe or a fully mobile probe, respectively, and is calculated from the central linewidth (ΔH_0 or δ):

$$M_s = \frac{(\delta_{exp}^{-1} - \delta_i^{-1})}{(\delta_m^{-1} - \delta_i^{-1})}$$

where δ_{exp} is the experimentally determined central linewidth of R1 at the site of interest and δ_i and δ_m are the corresponding values for the most immobile and most mobile sites observed, respectively. These values were set at 2.1 G for δ_m and 8.4 G for δ_i but are somewhat arbitrary and dependent on local polarity within the protein [35]. Relative values are, however, of primary importance when comparing mobilities at different sites.

To evaluate the structural environment of the spin-labeled side chains, the reciprocal of the central peak width (ΔH_0) and the reciprocal of the spectral second moment

($<H^2>$) are considered to be good measures. $<H^2>$ was determined for each spectrum according to a previously described method [46].

τ_R is another quantitative measure of nitroxide mobility. In the slow motion regime, τ_R can be calculated according to the ΔS method [47]:

$$\tau_R = a\left(1 - \left(\frac{2A_{zz}}{2A_{zz}^{max}}\right)\right)^b$$

where $2A_{zz}$ is the measured spectral width (defined as the distance between the outermost extrema) and $2A_{zz}^{max}$ is the maximum spectral width observed for the free MTS spin label, which is 75.8 G. The values of the constants a and b are dependent on the central linewidth (δ): for a spectrum with a 3.0 G central linewidth, the values are 5.4×10^{-10} and -1.36, respectively [48].

Acknowledgements

The authors would like to thank the University of Iceland Research Fund and the Icelandic Research Fund for financial support; Professor Einar Árnason at the Institute of Biology, University of Iceland, for access to DNA sequencing; Pavol Cekan for help with EPR measurements; and Professor Leslie Fung at the Chemistry Department, University of Chicago Illinois, for supplying the spreadsheet that allowed us to perform second moment calculations.

References

1 Hammes GG (2002) Multiple conformational changes in enzyme catalysis. *Biochemistry* **41**, 8221–8228.
2 Henzler-Wildman K & Kern D (2007) Dynamic personalities of proteins. *Nature* **450**, 964–972.
3 Henzler-Wildman KA, Lei M, Thai V, Kerns SJ, Karplus M & Kern D (2007) A hierarchy of timescales in protein dynamics is linked to enzyme catalysis. *Nature* **450**, 913–916.
4 Ishima R & Torchia DA (2000) Protein dynamics from NMR. *Nat Struct Biol* **7**, 740–743.
5 Kay LE (2005) NMR studies of protein structure and dynamics. *J Magn Reson* **173**, 193–207.
6 Englander JJ, Del Mar C, Li W, Englander SW, Kim JS, Stranz DD, Hamuro Y & Woods VL Jr (2003) Protein structure change studied by hydrogen-deuterium exchange, functional labeling, and mass spectrometry. *Proc Natl Acad Sci USA* **100**, 7057–7062.
7 Englander SW (2006) Hydrogen exchange and mass spectrometry: a historical perspective. *J Am Soc Mass Spectrom* **17**, 1481–1489.
8 Maragakis P, Lindorff-Larsen K, Eastwood MP, Dror RO, Klepeis JL, Arkin IT, Jensen MØ, Xu H, Trbovic N, Friesner RA *et al.* (2008) Microsecond molecular dynamics simulation shows effect of slow loop dynamics on backbone amide order parameters of proteins. *J Phys Chem B* **112**, 6155–6158.
9 Weiss S (2000) Measuring conformational dynamics of biomolecules by single molecule fluorescence spectroscopy. *Nat Struct Biol* **7**, 724–729.
10 Agarwal PK (2006) Enzymes: an integrated view of structure, dynamics and function. *Microb Cell Fact* **5**, 2.
11 Eisenmesser EZ, Millet O, Labeikovsky W, Korzhnev DM, Wolf-Watz M, Bosco DA, Skalicky JJ, Kay LE & Kern D (2005) Intrinsic dynamics of an enzyme underlies catalysis. *Nature* **438**, 117–121.
12 Agarwal PK (2005) Role of protein dynamics in reaction rate enhancement by enzymes. *J Am Chem Soc* **127**, 15248–15256.
13 Kern D, Eisenmesser EZ & Wolf-Watz M (2005) Enzyme dynamics during catalysis measured by NMR spectroscopy. *Methods Enzymol* **394**, 507–524.
14 Fanucci GE & Cafiso DS (2006) Recent advances and applications of site-directed spin labeling. *Curr Opin Struct Biol* **16**, 644–653.
15 Columbus L & Hubbell WL (2002) A new spin on protein dynamics. *Trends Biochem Sci* **27**, 288–295.
16 Hubbell WL, Mchaourab HS, Altenbach C & Lietzow MA (1996) Watching proteins move using site-directed spin labeling. *Structure* **4**, 779–783.
17 Trad CH, James W, Bhardwaj A & Butterfield DA (1995) Selective labeling of membrane protein sulfhydryl groups with methanethiosulfonate spin label. *J Biochem Biophys Methods* **30**, 287–299.
18 McHaourab HS, Lietzow MA, Hideg K & Hubbell WL (1996) Motion of spin-labeled side chains in T4 lysozyme. Correlation with protein structure and dynamics. *Biochemistry* **35**, 7692–7704.
19 Steinhoff HJ (2004) Inter- and intra-molecular distances determined by EPR spectroscopy and site-directed spin labeling reveal protein-protein and protein-oligonucleotide interaction. *Biol Chem* **385**, 913–920.
20 Zhou Z, DeSensi SC, Stein RA, Brandon S, Dixit M, McArdle EJ, Warren EM, Kroh HK, Song L, Cobb CE *et al.* (2005) Solution structure of the cytoplasmic domain of erythrocyte membrane band 3 determined by site-directed spin labeling. *Biochemistry* **44**, 15115–15128.
21 Vamvouka M, Cieslak J, Van Eps N, Hubbell W & Gross A (2008) The structure of the lipid-embedded potassium channel voltage sensor determined by double-electron-electron resonance spectroscopy. *Protein Sci* **17**, 506–517.
22 Hauksson JB, Andrésson ÓS & Ásgeirsson B (2000) Heat-labile bacterial alkaline phosphatase from a marine *Vibrio* sp. *Enzyme Microb Technol* **27**, 66–73.

23 Helland R, Larsen RL & Ásgeirsson B (2009) The 1.4 Å crystal structure of the large and cold-active *Vibrio* sp. alkaline phosphatase. *Biochim Biophys Acta, Proteins Proteomics* **1794**, 297–308.
24 Marx JC, Collins T, D'Amico S, Feller G & Gerday C (2007) Cold-adapted enzymes from marine Antarctic microorganisms. *Mar Biotechnol (NY)* **9**, 293–304.
25 Somero GN (2004) Adaptation of enzymes to temperature: searching for basic 'strategies'. *Comp Biochem Physiol* **139**, 321–333.
26 Siddiqui KS & Cavicchioli R (2006) Cold-adapted enzymes. *Annu Rev Biochem* **75**, 403–433.
27 Papaleo E, Riccardi L, Villa C, Fantucci P & De Gioia L (2006) Flexibility and enzymatic cold-adaptation: a comparative molecular dynamics investigation of the elastase family. *Biochim Biophys Acta, Proteins Proteomics* **1764**, 1397–1406.
28 Stec B, Holtz KM & Kantrowitz ER (2000) A revised mechanism for the alkaline phosphatase reaction involving three metal ions. *J Mol Biol* **299**, 1303–1311.
29 Zalatan JG, Fenn TD & Herschlag D (2008) Comparative enzymology in the alkaline phosphatase superfamily to determine the catalytic role of an active-site metal ion. *J Mol Biol* **384**, 1174–1189.
30 Hinberg I & Laidler KJ (1972) Steady-state kinetics of enzyme reactions in the presence of added nucleophiles. *Can J Biochem* **50**, 1334–1359.
31 Ásgeirsson B, Adalbjörnsson BV & Gylfason GA (2007) Engineered disulfide bonds increase active-site local stability and reduce catalytic activity of a cold-adapted alkaline phosphatase. *Biochim Biophys Acta* **1774**, 679–687.
32 Janeway CML, Xu X, Murphy JE, Chaidaroglou A & Kantrowitz ER (1993) Magnesium in the active site of *Escherichia coli* alkaline phosphatase is important for both structural stabilization and catalysis. *Biochemistry* **32**, 1601–1609.
33 Sun L, Martin DC & Kantrowitz ER (1999) Rate-determining step of *Escherichia coli* alkaline phosphatase altered by the removal of a positive charge at the active center. *Biochemistry* **38**, 2842–2848.
34 Guo Z, Cascio D, Hideg K, Kalai T & Hubbell WL (2007) Structural determinants of nitroxide motion in spin-labeled proteins: tertiary contact and solvent-inaccessible sites in helix G of T4 lysozyme. *Protein Sci* **16**, 1069–1086.
35 Columbus L & Hubbell WL (2004) Mapping backbone dynamics in solution with site-directed spin labeling: GCN4-58 bZip free and bound to DNA. *Biochemistry* **43**, 7273–7287.
36 Pace CN (1986) Determination and analysis of urea and guanidine hydrochloride denaturation curves. *Methods Enzymol* **131**, 266–280.
37 Isas JM, Langen R, Haigler HT & Hubbell WL (2002) Structure and dynamics of a helical hairpin and loop region in annexin 12: a site-directed spin labeling study. *Biochemistry* **41**, 1464–1473.
38 Pistolesi S, Ferro E, Santucci A, Basosi R, Trabalzini L & Pogni R (2006) Molecular motion of spin labeled side chains in the C-terminal domain of RGL2 protein: a SDSL-EPR and MD study. *Biophys Chem* **123**, 49–57.
39 Margittai M, Fasshauer D, Pabst S, Jahn R & Langen R (2001) Homo- and heterooligomeric SNARE complexes studied by site-directed spin labeling. *J Biol Chem* **276**, 13169–13177.
40 Gudjónsdóttir K & Ásgeirsson B (2008) Effects of replacing active site residues in a cold-active alkaline phosphatase with those found in its mesophilic counterpart from *Escherichia coli*. *FEBS J* **275**, 117–127.
41 Moffat JK (1971) Spin-labelled haemoglobins: a structural interpretation of electron paramagnetic resonance spectra based on X-ray analysis. *J Mol Biol* **55**, 135–146.
42 Guo Z, Cascio D, Hideg K & Hubbell WL (2008) Structural determinants of nitroxide motion in spin-labeled proteins: solvent-exposed sites in helix B of T4 lysozyme. *Protein Sci* **17**, 228–239.
43 Ásgeirsson B & Andrésson ÓS (2001) Primary structure of cold-adapted alkaline phosphatase from a *Vibrio* sp. as deduced from the nucleotide gene sequence. *Biochim Biophys Acta* **1549**, 99–111.
44 Zaman Z & Verwilghen RL (1979) Quantitation of proteins solubilized in sodium dodecyl sulfate-mercaptoethanol-tris electrophoresis buffer. *Anal Biochem* **100**, 64–69.
45 Pace CN, Vajdos F, Fee L, Grimsley G & Gray T (1995) How to measure and predict the molar absorption coefficient of a protein. *Prot Sci* **4**, 2411–2424.
46 Slichter CP (1996) *Principles of Magnetic Resonance*, Series: Springer Series in Solid-state Sciences, Vol. 1. Springer-Verlag, Berlin.
47 Freed JH (1976) Theory of slow tumbling ESR spectra for nitroxides. In *Spin Labeling: Theory and Application* (Berliner LJ, ed.), pp. 53–132. Academic Press, New York, NY.
48 Edwards TE, Robinson BH & Sigurdsson ST (2005) Identification of amino acids that promote specific and rigid TAR RNA-tat protein complex formation. *Chem Biol* **12**, 329–337.
49 Delano WL (2002) *The PyMOL Molecular Graphics System*. Delano Scientific, San Carlos, CA.